E. SUPPLEMENTARY MATERIAL — PART E

$\mathbf{Li^+}$–$\mathbf{H_2(D_2)}$

versus

$\mathbf{He^+}$–$\mathbf{H_2(D_2)}$

Fig. E1. Electronic structure input
to calculations on dynamics of the systems

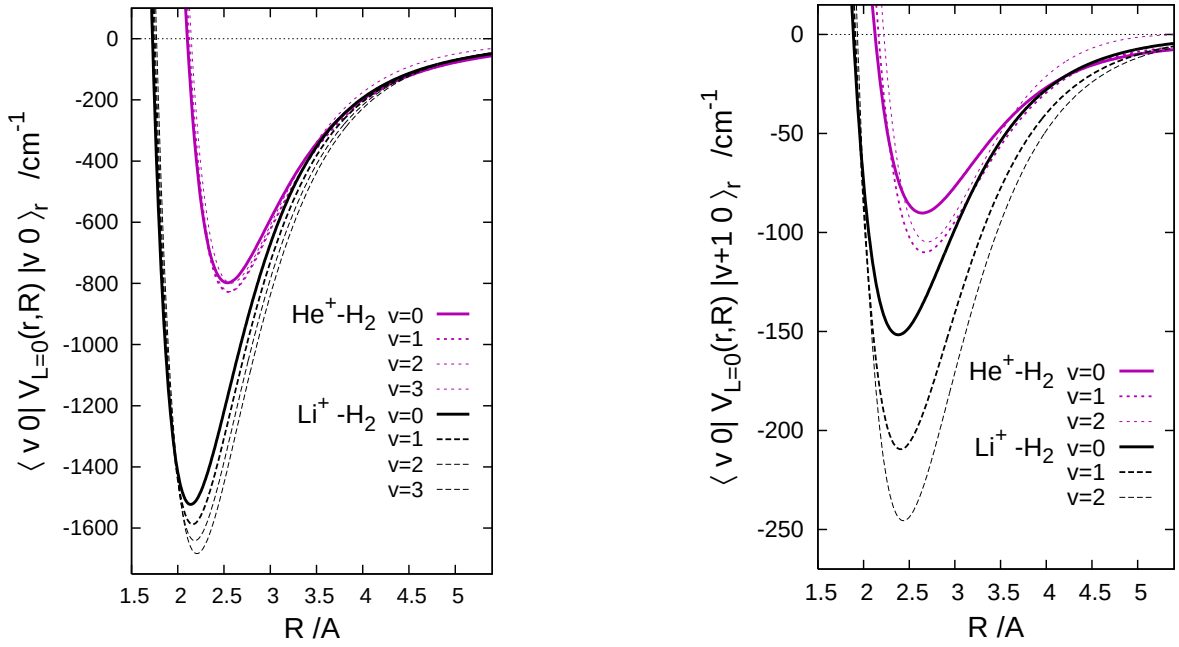

Potential energy surfaces for the a^+-H_2 systems with a=He and a=Li[♯]. The strength functions $V_L(r,R)$ resulting from the Legendre-polynomial expansions of the interaction potentials

$$\overline{V}^{i^+\text{-}H_2}(r,R,\theta) - \overline{V}^{i^+\text{-}H_2}(r,R{\to}\infty) = \sum_{L}^{L^{i}_{max}} V_L^{i^+\text{-}H_2}(r,R)\, P_L(\cos\theta)$$

for i=He, Li. L^{Li}_{max}=10 and L^{He}_{max}=4.

E1a. Average values of the L=0-strength functions in four lowest vibrational states of H_2.

E1b. Matrix elements of the potential functions $V_{L=0}(r,R)$ between v and v+1 vibrational functions of H_2 for v=0–2.

[♯]The He^+–H_2 complex is formed on the PES of the first excited electronic state of the $[HeHH]^+$ system. The respective part of this PES is taken from Ref. 1.

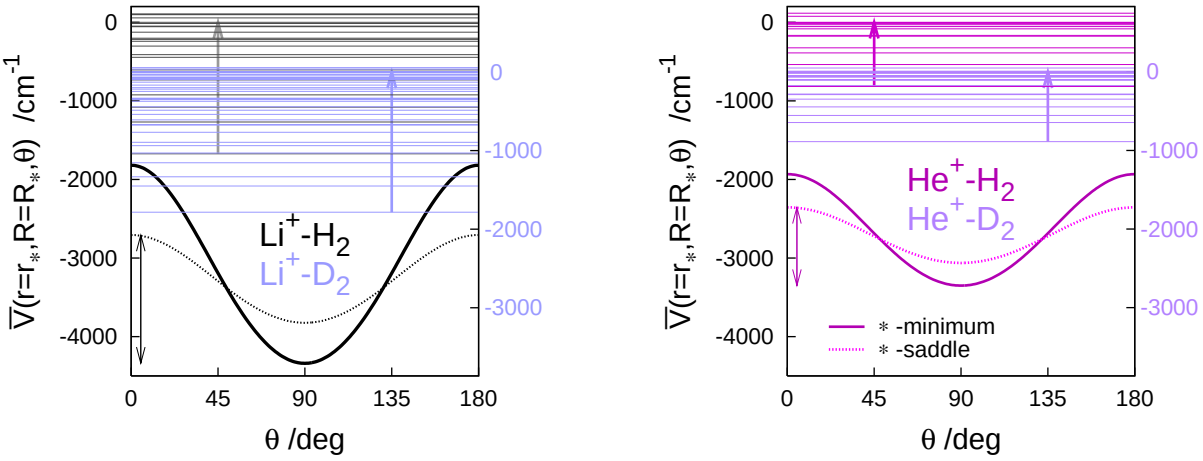

E1c. Fig. 1a of the paper, presenting 1D cuts of the PES of the ground electronic state of $[LiHH]^+$ through the minimum and saddle points and the location of the J=0 bound state energy levels of the complexes Li^+–$H_2(D_2)$, is compared here with the analogous cuts of the PES of the first excited electronic state of $[HeHH]^+$ and the location on this PES of the levels of the He^+–$H_2(D_2)$ complexes. The double arrows show the barriers to linearity on the PESs, the single arrows — the dissociation energies of the complexes.

Fig. E2. Energies of $v_r\, b\, k\, J{=}k$ states for $v_r{=}0, 1$ ($v_r{\sim}v$, $b{\sim}j$)

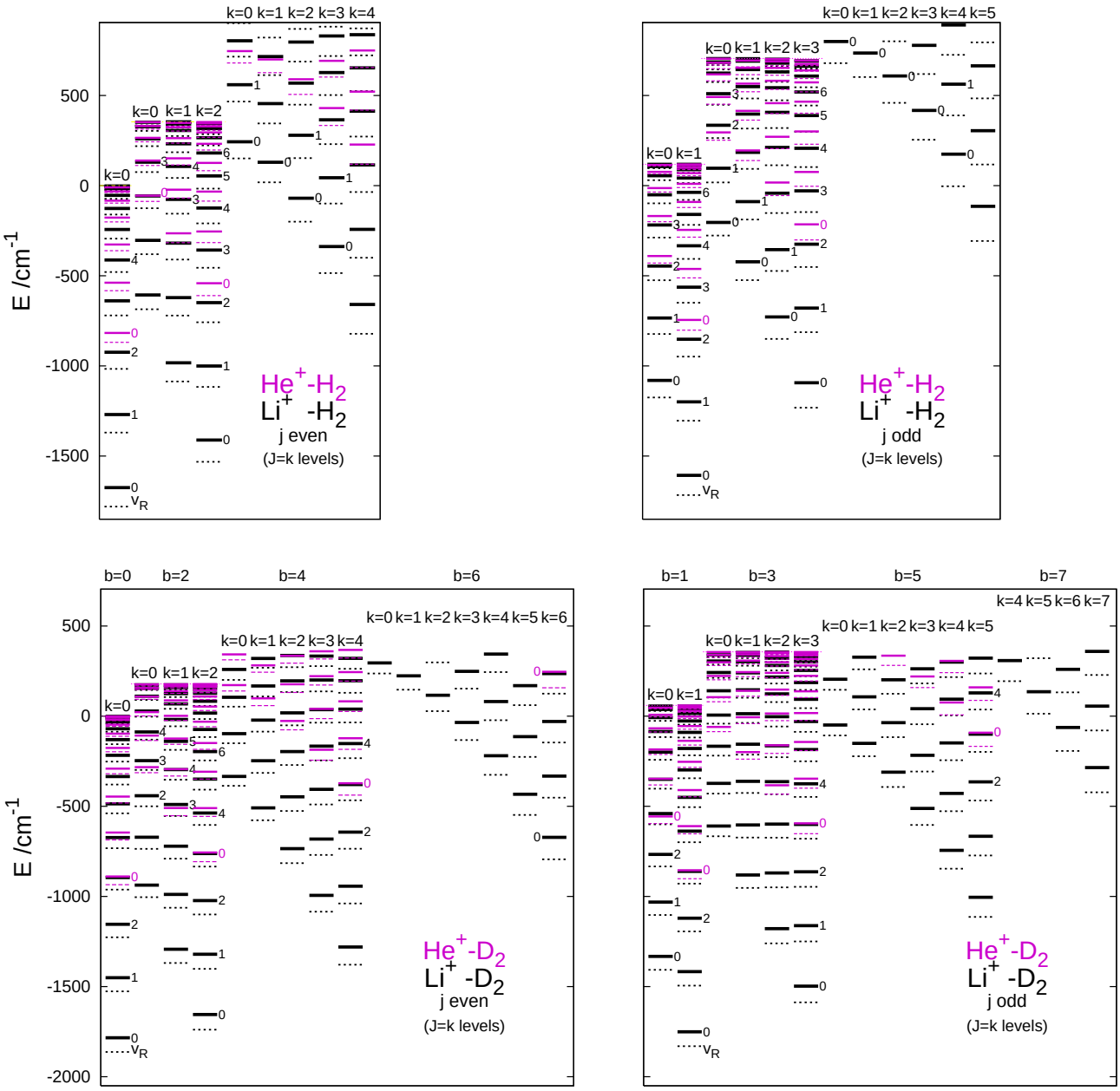

The energies of $v_r{=}0$ and $v_r{=}1$ states, shown with continuous and broken lines, respectively, are relative to the $v{=}v_r\, j{=}0$ dissociation thresholds of the complexes. The $v{=}1\, j{=}0$ thresholds are shifted down to coincide with $v{=}0\, j{=}0$. Each line in $k{>}0$ ladders represents two states, of e- and f-parity.

The energies of the He^+–H_2 complex come from calculations of Refs. 3 and 4, see Tables CII and CIII in the later paper. Information on states of the He^+–D_2 complex was generated in this work. In numerical form, it is presented in Tables EI and EII at the end of this file.

The topological similarity of the PESs of the ground electronic states of the $LiHH^+$ and the first excited state of the $HeHH^+$ in their lowest parts, pointed out in Ref. 2 and illustrated here in Fig. E1, is a good reason to expect that ro-vibrational dynamics on these PESs is similar, too. In particular, bound and quasi-bound rovibrational states on the PESs constituting the Li^+–H_2 and He^+–H_2 complexes should reveal qualitatively the same features.

This part of the supplementary material has in goal to document the qualitative similarity and the quantitative differences between the complexes in the following aspects of their dynamics:

(i) bound and quasi-bound states associated with v=0 j and v=1 j thresholds, structures of vibrational energy levels in the ranges up to the positions of j=3 limits,

(ii) vibrational predissociation; rates of the process from different states, correlations with quantum numbers characterizing the states, effects of the H→D substitution; propensities in populations of decay channels.

Fig. E2 and Tables EI–EII concern aspect (i). Because of the nearly two times shallower potential well, the ro-vibrational spectra of the He^+–$H_2(D_2)$ complexes contain much less levels than the spectra of the Li^+–$H_2(D_2)$ complexes in the same ranges. For example, there are 100 'vibrational' (J=k) bound-state levels in the spectrum of the He^+–D_2 complex while 218 such levels occur in the spectrum of Li^+–D_2. As to 'vibrational' quasi-bound states associated with the v=1 thresholds which can decay by pure vibrational predissociation: 99 such states (widths listed in red in Tables EI–EII) are found in the He^+–D_2 complex and above twice as many (232) — in the Li^+–D_2 complex, cf. Tables CI–CII in Part C.

Figs. E3–E6 concern aspect (ii). The findings are detailed in the caption texts and in the comments to these figures. Worth of pointing out here seems the finding which concern the isotopic substitution effects on the vibrational predissociation widths, on their size and their dependencies on the quantum numbers characterizing the decaying states. The simple scaling factors that reasonably account for differences in these respects between the Li^+–H_2 and Li^+–D_2 complexes (cf. Figs. 8d and 10b in the paper) can, to a considerable degree, be rationalized by inspection of results of the perturbative 3D-CM calculations (Fig. D14 in Part D of this material). Still, the concrete forms of these factors should be regarded as (at most semi-) empirical. It is therefore reassuring to see that factors of the same forms do also reasonably account for effects of the H→D substitution on the vibrational predissociation characteristics of the He^+–H_2 complex, i.e. a complex about 10 times more stable than Li^+–H_2 against decay by this mechanism.

Vibrational predissociation (VP)

⋮

⋮

Fig. E3. Total widths of $[v_r{=}1\, v_\theta\, v_R]\, k\, J{=}k$ states

Populations (Γ_j/Γ) of decay channels $D_2(v{=}0\, j)$ + $Li^+(He^+)$

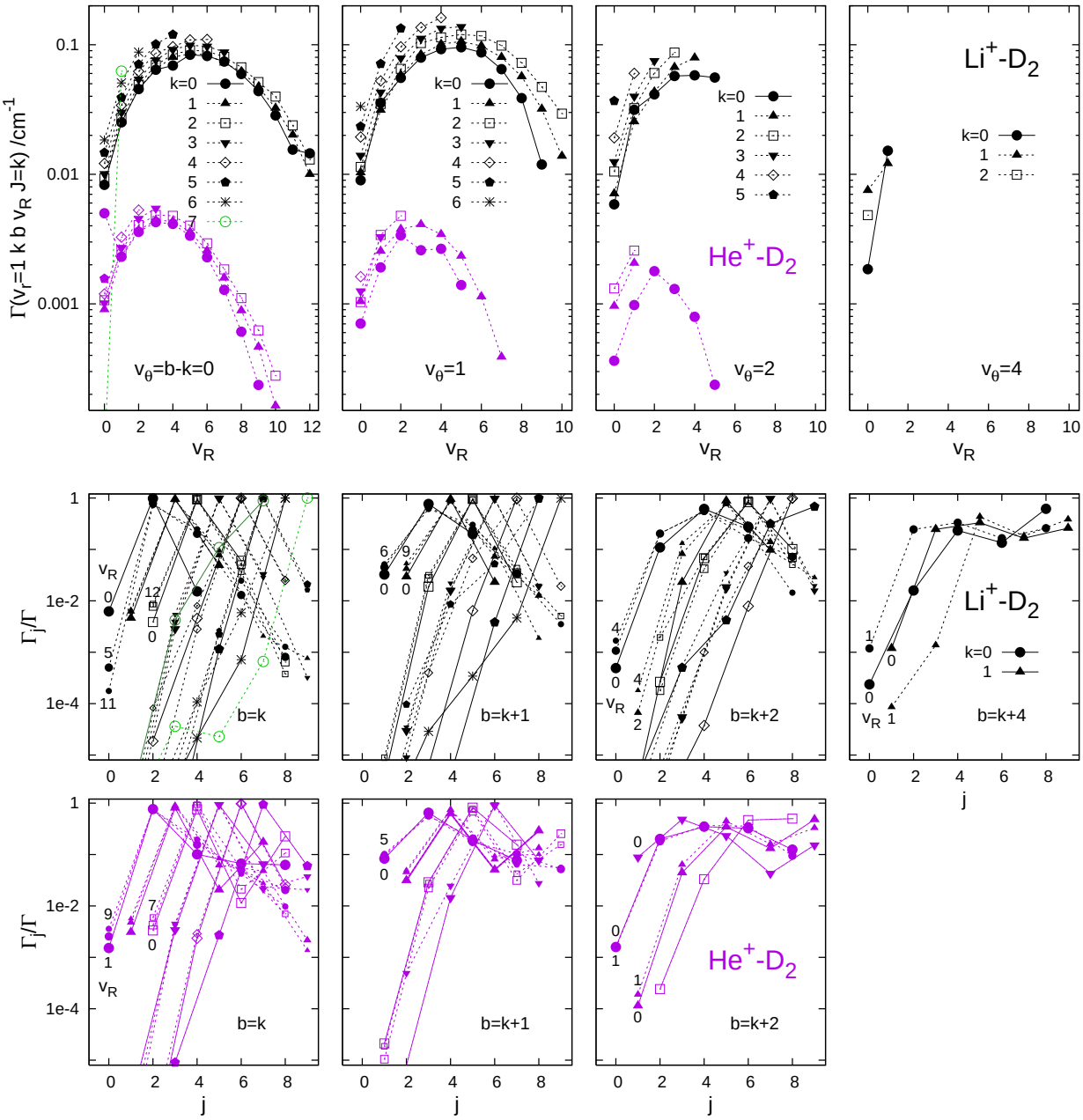

The widths are shown for states which can decay only by VP (no admixture of rotational predissociation to $v{=}1\, j$ channels). For $k{>}0$, states of f-parity are shown. The symbols in the Γ_j/Γ panels denote the values of k as specified in the panels of the upper row. The data for the two states $b{=}k{=}J{=}7\, v_R{=}0, 1$ of the Li^+–D_2 complex are shown with different (green) color to stress the fact that the exceptional smallness of the width Γ of the lower of these states is also a manifestation of the $b{\to}j{=}b{+}2$ propensity in the population of decay channels. Namely, the most probable j channel for decay of this state, $j{=}9$, is closed.

In the upper panels of Fig. E3, the total VP widths of lowest rotational levels ($J{=}k$) in different groups k of vibrational states $[v_r{=}1\, v_\theta\, v_R]$ of the complex Li^+–D_2 are compared with the total VP widths of analogous levels of the complex He^+–D_2 and demonstrated to be about 10 times bigger. This comes mostly from the different strength of the r-dependence of the respective PESs which is illustrated in Fig. E1b.

The comparison of the partial VP widths in the panels of the middle and bottom rows of Fig. E3 reveals that:
(i) In the VP of both complexes from their states with low v_θ ($\leq$1), the propensity: max Γ_j/Γ at $j{=}b{+}2$, holds with comparable strength.
(ii) The $b{\to}j{=}b{+}2$ propensity weakens and the tendency to populate the highest open j channel appears when the predissociating states are excited in the bending mode. The only difference between the two complexes is the value of the quantum number v_θ of the state for which this change becomes visible — an obvious consequence of the different binding energies (Fig. E1a) and the different barriers (Fig. E1c) that hinder rotations of the D_2 subunit within the complexes.

Qualitatively the same in both complexes, Li^+–D_2 and He^+–D_2, are the dependencies of the total VP widths on the quantum numbers v_R, v_θ, and v_r (the latter shown in Fig. E4b). Also, the effect on the widths of replacing the D_2 subunit with H_2 appears describable in the same way, as demonstrated in both parts of the figure below. Worth of noting is, however, the quantitative difference which is displayed in Fig. E4b. Namely, the proportionality to v_r^2 is better fulfilled by the widths of the complexes with the He^+ ion. This should be attributed to the weaker $r-R$ dependence of the PES which is shown in Fig. E1 (by the smaller changes of the averages $\langle v|\ldots|v\rangle_r$ and $\langle v|\ldots|v{+}1\rangle_r$ with increasing v).

Fig. E4. Widths of $[v_r{=}1{-}3\, v_\theta{=}0\, v_R]\, k\, J{=}k$ states

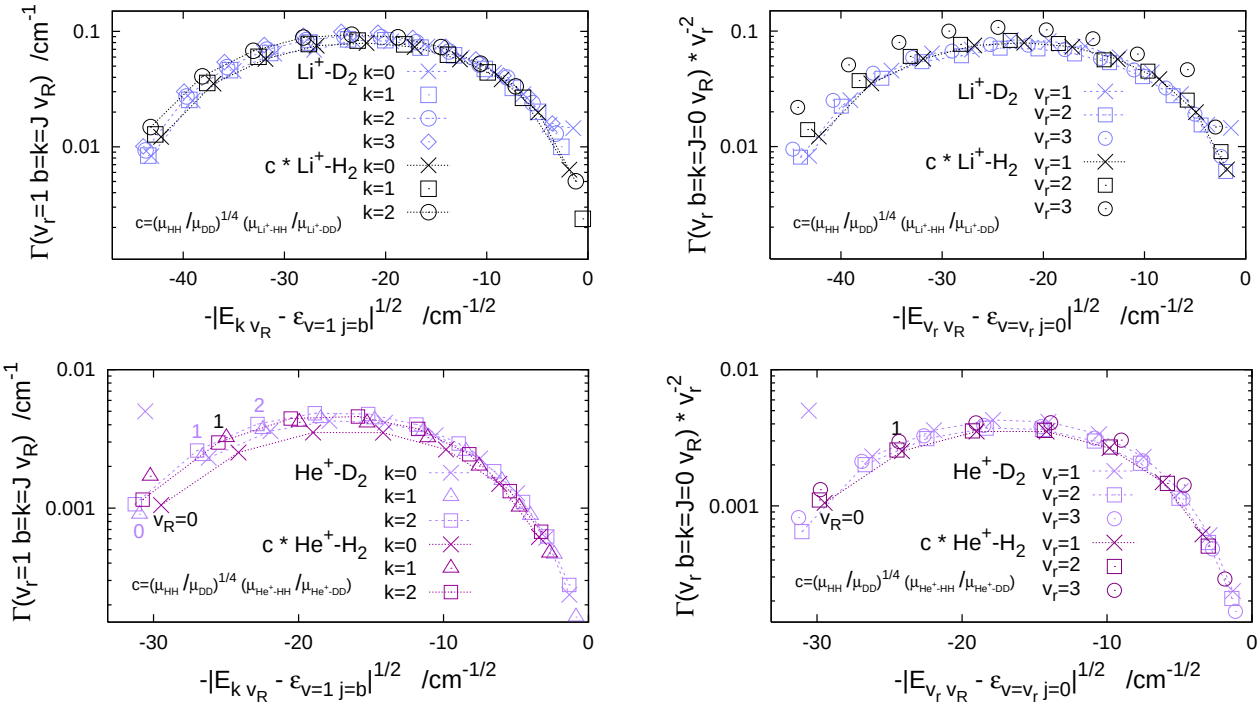

E4a. Widths $\Gamma([v_r{=}1\, v_\theta{=}0\, v_R]\, k\, J{=}k)$ as functions of $-|E_{k\, v_R}{-}\varepsilon_{v=1\, j=b}|^{1/2}$, where $E_{k\, v_R}{:=}E([v_r{=}1\, v_\theta{=}0\, v_R]k\, J{=}k)$.

E4b. A demonstration of v_r^2-dependence of the VP widths on the vibrational quantum number of the diatomic subunit of the complexes. $E_{v_r\, v_R}{:=}E([v_r\, v_\theta{=}0\, v_R]k{=}J{=}0)$.

Approximate scaling of the widths upon the D→H substitution. The scaling factor $c{=}\left(\frac{\mu_{\rm HH}}{\mu_{\rm DD}}\right)^{1/4}\frac{\mu_{\rm i^+-HH}}{\mu_{\rm i^+-DD}}$ takes the values of 0.5145 and 0.5616 for $i^+{=}Li^+$ and $i^+{=}He^+$, respectively.

Fig. E5. Vibrational predissociation widths of J-levels in k=0–3 groups of states $[v_r{=}1\, v_\theta{=}0\, v_R{=}0{-}1]$

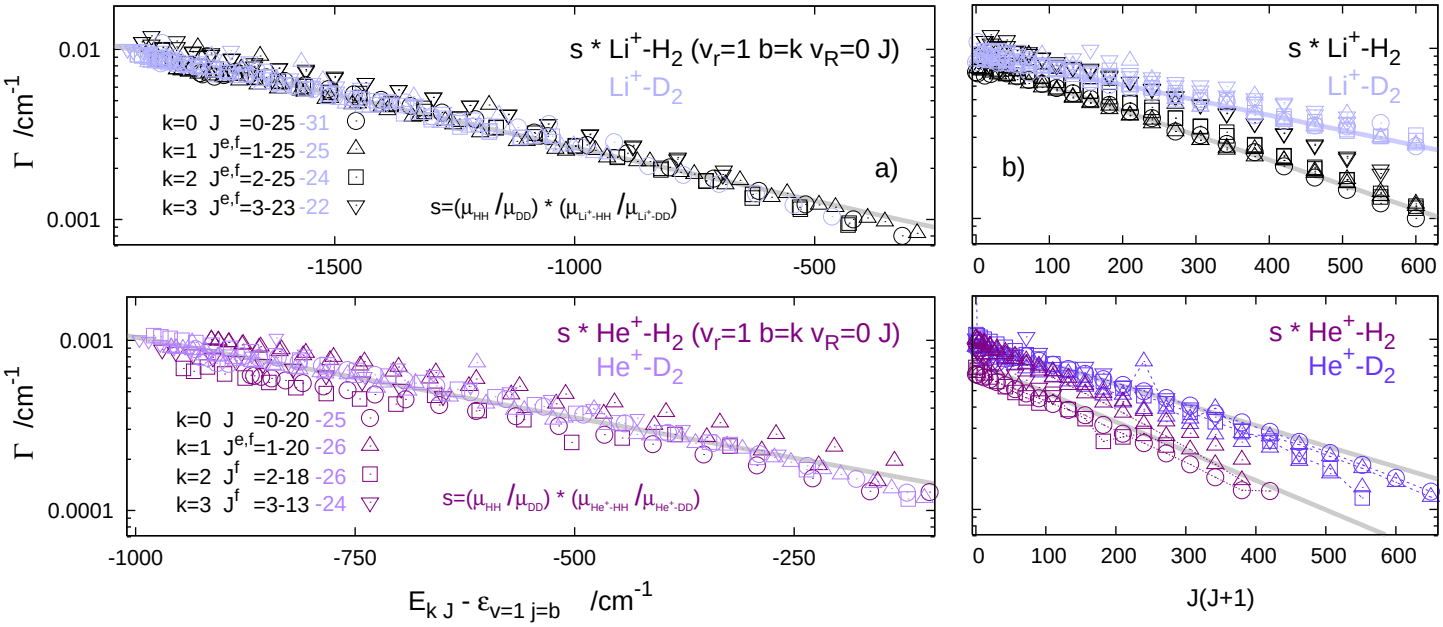

a) The VP widths $\Gamma([v_r{=}1\, v_\theta{=}0\, v_R{=}0]\, k\, J)$ of the Li^+–$H_2(D_2)$ and He^+–$H_2(D_2)$ complexes as functions of energies of the states relative to the $v{=}1\ j{=}b$ thresholds, $E_{k\,J}{-}\varepsilon_{v=1\,j=b}$, where $E_{k\,J}{:=}E([v_r{=}1\, v_\theta{=}0\, v_R{=}0]\, k\, J)$. Approximate scaling of the widths upon the H→D substitution, $\Gamma^{i^+-DD} \approx s{\times}\Gamma^{i^+-HH}$ where the factor $s{=}\frac{\mu_{HH}}{\mu_{DD}}\frac{\mu_{i^+-HH}}{\mu_{i^+-DD}}$ is 0.3060 and 0.3341 for the complexes with the ion $i^+{=}Li^+$ and He^+, respectively.

b) The widths as functions of the number $J(J{+}1)$. Effects of the isotopic substitution on these functions are not as simple as on the functions shown in part a) of the figure. Namely, the lines that pertain to complexes formed by H_2 have different slopes than the lines pertaining to complexes formed by D_2. The slopes are nearly proportional to inverses of the reduced masses of the respective complexes.

Below: Same as a) and b) for widths $\Gamma([1\,0\,v_R{=}1]\, k\, J)$ of the four complexes $i^+{-}a_2$ for i=He,Li and a=H,D.

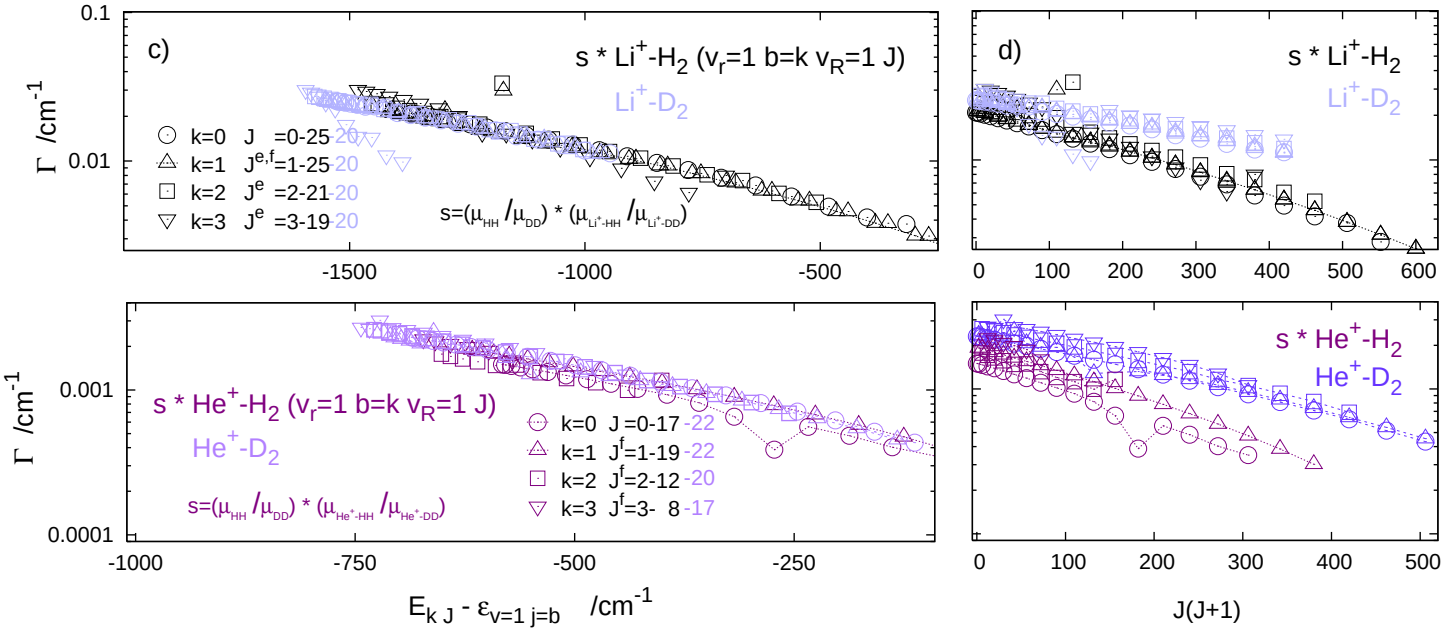

Fig. E6. Vibrational predissociation widths of J-levels in states with excited bending vibrations

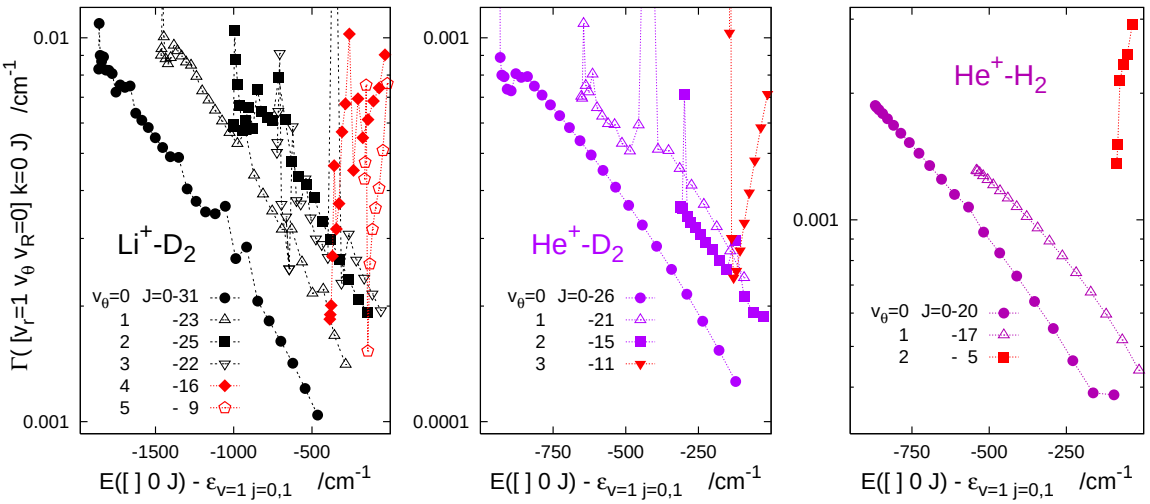

E6a. Total widths Γ of states $[v_r{=}1\, v_\theta\, v_R{=}0]\, k{=}0\, J$ of the complexes Li^+–D_2, He^+–D_2 and He^+–H_2 presented as functions of energy of J levels relative to the threshold $v{=}1\, j$ with $j{=}0\,(1)$ for even (odd) values of v_θ. The functions $\Gamma_{v_\theta}(E(J))$ are plotted for the v_θ's and ranges of J specified for each complex in the respective panel of the figure.

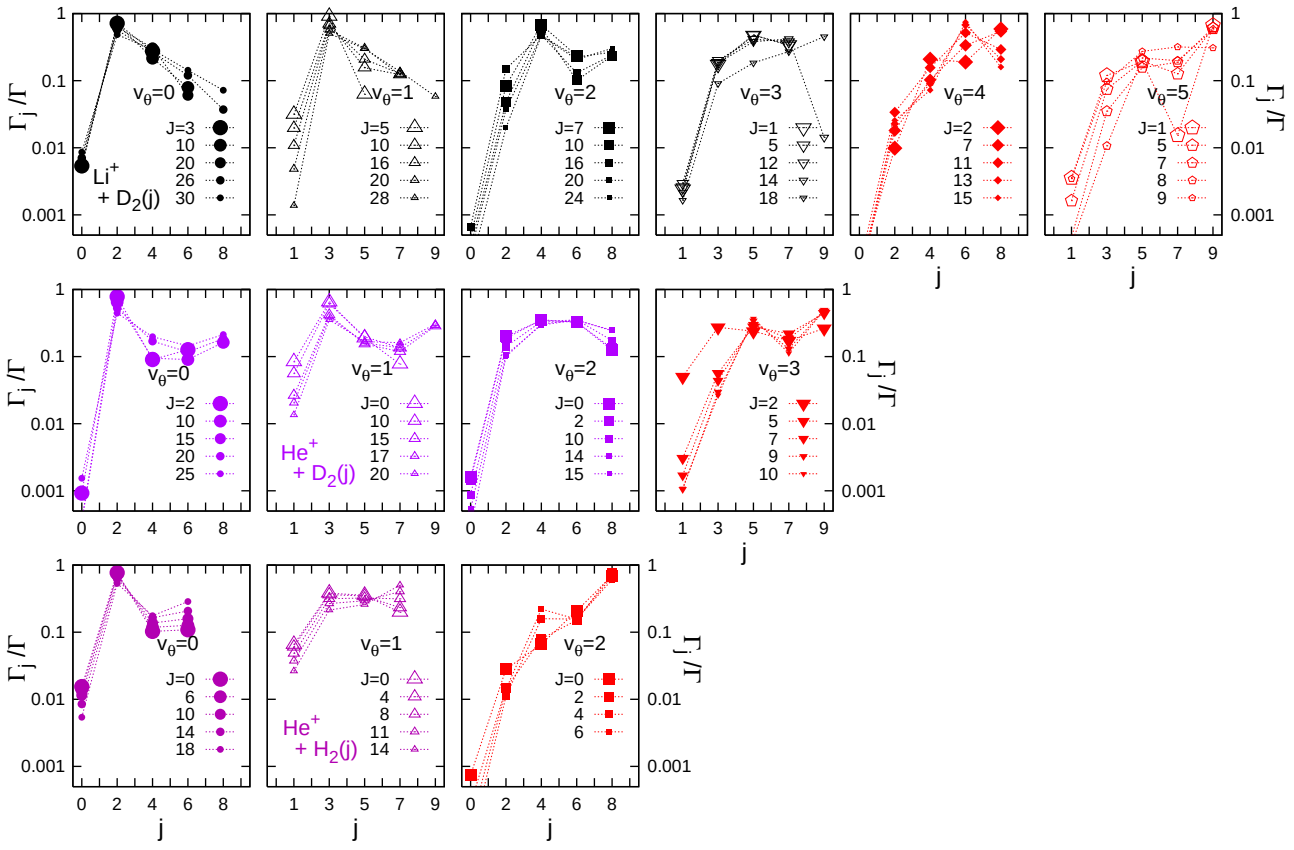

E6b. Widths $\Gamma_{v_\theta}(E(J))$ — points of the curves from Fig. E6a at selected values of J — resolved into partial widths giving the populations of decay channels $Li^+{+}D_2(v{=}0, j)$ and $He^+{+}a_2(v{=}0, j)$ for a=H,D.

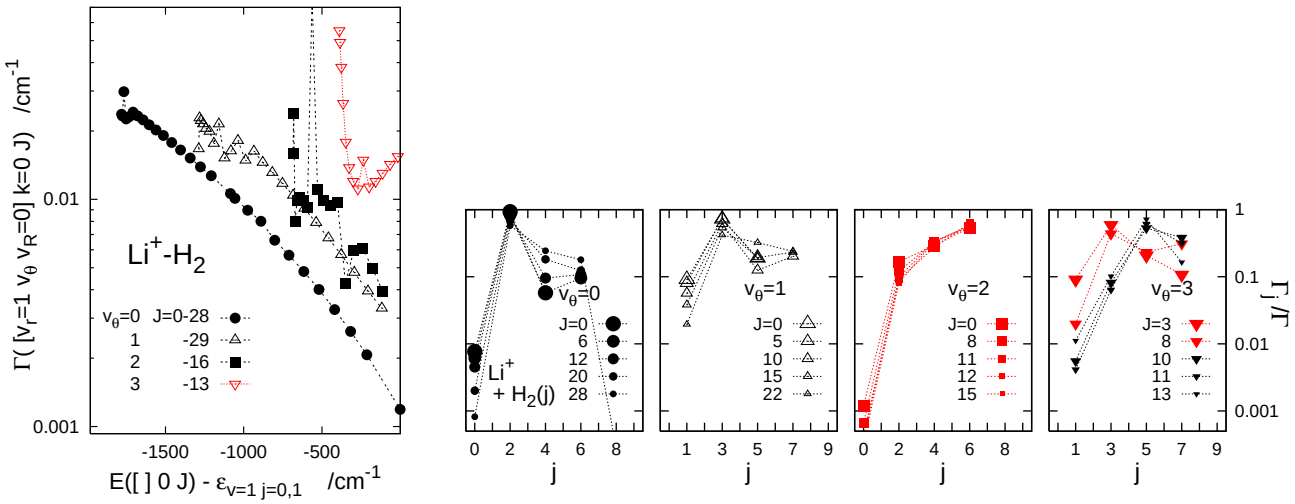

E6c and **E6d**. Same as E6a and E6b, respectively, for the Li^+-H_2 complex.

COMMENT

In all parts of Fig. E6 some curves are drawn in red with the intention of calling attention to the presumably existing correlation between the change in the character of the total VP widths as functions of the number J and the change in the relative magnitude of the partial widths for decay to different available j channels. Such correlation was noted in the VP of the Li^+–D_2 complex from its v_θ=4, 5 states, cf. Fig. D13 in Ref. 6. Here, in panels E6a and E6b, it can also be observed in the decay of the complexes He^+–D_2 and He^+–H_2 from their excited states v_θ=3 and v_θ=2. However, despite this evidence the correlation not necessarily always shows up. An example is the case of the Li^+–H_2 complex predissociating from its rotational levels in the state [1 2 0], presented in panels E6c and E6d. The partial widths clearly violate the $b(:=v_\theta+k)$=2→j=4 propensity but the total widths still behave 'normally', i.e. they decrease with growing J.

TABLE EI: He^+–D_2(I=0, 2). Positions (E) and widths (Γ) of 'vibrational' levels (b=$j\,k\,v_R$ J=k p) below the v=0–1 j=0–6 thresholds. The positions are relative to the respective $v\,j$=0 threshold. The positions of j>0 thresholds are shown in lines marked with ε [a]. All data are in cm^{-1}.

			v=0 (ε=0)				v=1 (ε=2986.41)			
			p=1		p=−1		p=1		p=−1	
j	k	v_R	E	Γ^a	$E-E(p{=}1)$	Γ^b	E	Γ^b	$E-E(p{=}1)$	Γ^c
0	0	0	−889.03	0			−934.57	5.0 (−3)		
		1	−645.11	0			−686.02	2.3 (−3)		
		2	−446.07	0			−481.28	3.6 (−3)		
		3	−290.58	0			−319.16	4.3 (−3)		
		4	−175.81	0			−197.20	4.1 (−3)		
		5	−96.88	0			−111.33	3.4 (−3)		
		6	−47.16	0			−55.90	2.3 (−3)		
		7	−19.39	0			−24.20	1.3 (−3)		
		8	−6.09	0			−8.56	6.1 (−4)		
		9	−0.79	0			−1.73	2.4 (−4)		
2	2	0	−755.91	0	0.00	0	−806.82	1.1 (−3)	0.00	1.1 (−3)
		1	−509.52	0	0.00	0	−556.03	2.6 (−3)	0.00	2.6 (−3)
		2	−307.73	0	0.00	0	−348.84	4.1 (−3)	0.00	4.1 (−3)
		3	−149.02	0	0.00	0	−183.90	4.8 (−3)	0.00	4.8 (−3)
		4	−30.32	0	0.00	0	−58.51	4.8 (−3)	0.00	4.8 (−3)
		5	53.50	7.3 (−5)	0.00	0	31.66	4.1 (−3)	0.00	4.0 (−3)
		6	108.91	4.8 (−5)	0.00	0	92.39	3.0 (−3)	0.00	2.9 (−3)
		7	142.93	2.1 (−5)	0.00	0	130.22	1.9 (−3)	0.00	1.8 (−3)
		8	162.38	1.8 (−5)	0.00	0	152.14	1.1 (−3)	0.00	1.1 (−3)
		9	173.05	1.1 (−5)	0.00	0	164.42	6.4 (−4)	0.00	6.2 (−4)
		10	178.13	1.1 (−5)	0.00	0	170.75	2.9 (−4)	0.00	2.8 (−4)
2	1	0	−509.25	0	0.14	0	−551.76	1.0 (−3)	0.13	1.0 (−3)
		1	−294.02	0	0.16	0	−332.06	2.6 (−3)	0.14	2.6 (−3)
		2	−123.94	0	0.14	0	−156.16	3.8 (−3)	0.13	3.8 (−3)
		3	2.12	2.6 (−3)	0.14	0	−23.24	3.8 (−3)	0.09	4.1 (−3)
		4	87.79	1.8 (−3)	0.13	0	69.39	5.6 (−3)	0.12	3.4 (−3)
		5	139.96	1.1 (−3)	0.12	0	127.06	3.6 (−3)	0.11	2.3 (−3)
		6	166.70	4.7 (−4)	0.10	0	157.26	1.7 (−3)	0.10	1.1 (−3)
		7	176.84	1.7 (−4)	0.12	0	169.36	3.7 (−4)	-0.09	3.9 (−3)
2	0	0	−282.42	0			−313.24	3.6 (−4)		
		1	−107.43	0			−134.43	9.8 (−4)		
		2	22.57	2.4 (−5)			1.41	1.8 (−3)		
		3	108.52	2.0 (−4)			93.85	1.3 (−3)		
		4	156.21	2.2 (−4)			147.80	7.9 (−4)		
		5	176.79	5.8 (−5)			168.61	2.4 (−4)		
ε			178.96				172.52			

TABLE EI: continued

4	4	0	−372.08	0	0.00	0	−437.74	1.2 (−3)	0.00	1.2 (−3)
		1	−122.43	0	0.00	0	−183.80	3.3 (−3)	0.00	3.3 (−3)
		2	82.68	3.1 (−9)	0.00	0	26.52	5.3 (−3)	0.00	5.3 (−3)
		3	244.86	4.7 (−4)	0.00	4.7 (-4)	194.71	7.0 (−3)	0.00	7.0 (−3)
		4	367.71	8.7 (−3)	0.00	8.6 (-3)	322.81	1.2 (−2)	0.00	1.1 (−2)
4	3	0	−186.00	0	0.00	0	−244.01	1.2 (−3)	0.00	1.3 (−3)
		1	40.49	6.6 (−8)	0.00	0	−13.38	3.3 (−3)	0.00	3.3 (−3)
		2	221.87	7.6 (−3)	0.00	7.8 (-3)	173.27	1.3 (−2)	0.00	1.3 (−2)
		3	359.81	8.7 (−3)	0.00	8.5 (-3)	317.35	1.5 (−2)	0.00	1.5 (−2)
4	2	0	−26.16	0	0.01	0	−75.58	7.7 (−3)	0.01	1.3 (−3)
		1	177.44	6.0 (−5)	-0.10	0	131.68	2.1 (−2)	0.01	2.6 (−3)
		2	335.01	4.2 (−2)	0.01	3.8 (-2)	294.22	3.8 (−3)	0.01	3.5 (−2)
4	1	0	97.89	4.1 (−7)	1.15	0	57.70	9.6 (−4	0.89	1.9 (−4)
		1	280.92	2.8 (−1)	0.90	1.2 (-1)	243.43	1.9 (= 1	0.76	6.5 (−2)
4	0	0	172.27	9.7 (−6)			140.15	3.6 (−5)		
		1	343.13	2.1			312.92	1.2		
ε			593.35				571.94			
6	6	0	246.37	3.2 (−8)	0.00	3.2 (-8)	157.77	1.9 (−3)	0.00	1.9 (−3)
ε			1235.73				1190.99			

[a]The positions of the thresholds listed here and in the following table are obtained from the asymptotic part of the used PES for the $HeHH^+$ system. In comparison with accurate values of $\varepsilon_{v\,j}-\varepsilon_{0\,0}$ for D_2[5], the positions are too low by values ranging from 0.04 to 0.79 cm^{-1} for v=0 j=1 − 6 and by 7.2 to 8.9 cm^{-1} for v=1 j=0–6. The latter shifts, rather large, indicate that the present PES, in particular its dependence of the r-coordinate, is much less accurate than the PES used in the calculations on the Li^+–H_2 (D_2) complexes. Still, it is believed that this fact have not exerted any severe impact on the comparisons presented in this file.

[b]All Γ>0 widths in the column are due to rotational predissociation.

[c]The red numbers in the column are widths due to pure vibrational predissociation (p=1 states of $E<\varepsilon_{10}$ and p=−1 states of $E<\varepsilon_{12}$).

TABLE EII: He^+–D_2(I=1). Positions (E) and widths (Γ) of 'vibrational' levels (b=$j\,k\,v_R$ J=k p) below the v=0–1 j=1–3 thresholds. The positions are relative to the respective $v\,j$=0 threshold[a]. The positions of j>0 thresholds are shown in lines marked with ε. All data are in cm^{-1}.

			v=0 (ε=0)				v=1 (ε=2986.41)			
			p=1		p=−1		p=1		p=−1	
j	k	v_R	E	Γ^a	$E-E(p=1)$	Γ^b	E	Γ^b	$E-E(p=1)$	Γ^c
1	1	0	−854.85	0	0.08	0	−901.78	9.0 (−4)	0.09	9.0 (−4)
		1	−610.06	0	0.08	0	−652.48	2.4 (−3)	0.08	2.4 (−3)
		2	−409.96	0	0.07	0	−446.84	3.7 (−3)	0.07	3.7 (−3)
		3	−253.10	0	0.05	0	−283.57	4.4 (−3)	0.06	4.4 (−3)
		4	−136.46	0	0.04	0	−160.06	4.3 (−3)	0.05	4.3 (−3)
		5	−54.97	0	0.03	0	−72.01	3.6 (−3)	0.03	3.6 (−3)
		6	−1.96	0	0.03	0	−13.60	2.6 (−3)	0.03	2.6 (−3)
		7	29.69	0	0.02	0	21.86	1.6 (−3)	0.02	1.6 (−3)
		8	47.03	0	0.01	0	41.56	8.9 (−4)	0.01	8.9 (−4)
		9	55.95	0	0.01	0	52.02	4.6 (−4)	0.01	4.6 (−4)
		10	59.53	0	0.01	0	56.84	1.6 (−4)	0.01	1.6 (−4)
1	0	0	−555.89	0			−595.32	7.0 (−4)		
		1	−347.36	0			−381.55	1.9 (−3)		
		2	−184.58	0			−212.14	3.4 (−3)		
		3	−67.20	0			−87.47	2.6 (−3)		
		4	7.98	0			−3.98	2.7 (−3)		
		5	47.85	0			41.71	1.4 (−3)		
ε			59.74				57.60			
3	3	0	−594.32	0	0.00	0	−651.53	9.7 (−4)	0.00	1.0 (−3)
		1	−346.23	0	0.00	0	−399.11	2.9 (−3)	0.00	2.7 (−3)
		2	−142.71	0	0.00	0	−190.29	4.6 (−3)	0.00	4.6 (−3)
		3	17.67	0	0.00	0	−23.78	5.5 (−3)	0.00	5.5 (−3)
		4	138.35	4.4 (−5)	0.00	4.4 (−5)	103.40	5.5 (−3)	0.00	5.5 (−3)
		5	224.10	4.2 (−5)	0.00	4.2 (−5)	195.40	4.7 (−3)	0.00	4.7 (−3)
		6	281.35	3.4 (−5)	0.00	3.4 (−5)	257.95	3.5 (−3)	0.00	3.5 (−3)
		7	317.03	2.4 (−5)	0.00	2.4 (−5)	297.52	2.3 (−3)	0.00	2.3 (−3)
		8	337.89	1.4 (−5)	0.00	1.4 (−5)	320.90	1.4 (−3)	0.00	1.4 (−3)
		9	349.68	1.6 (−5)	0.00	1.6 (−5)	334.34	8.0 (−4)	0.00	8.0 (−4)
		10	355.65	3.8 (−4)	0.00	1.4 (−5)	341.62	7.7 (−4)	0.00	4.0 (−4)
3	2	0	−383.03	0	0.00	0	−432.06	9.7 (−4)	0.00	1.0 (−3)
		1	−161.53	0	0.00	0	−206.41	3.4 (−3)	0.06	3.4 (−3)
		2	14.86	0	0.00	0	−24.50	4.8 (−3)	0.00	4.8 (−3)
		3	147.81	1.2 (−2)	0.06	7.2 (−3)	115.41	2.5 (−4)	0.28	8.9 (−3)
		4	240.22	2.1 (−3)	0.00	2.1 (−3)	213.81	7.6 (−3)	-0.01	7.4 (−3)
		5	299.60	1.4 (−3)	0.03	1.6 (−3)	278.61	5.1 (−3)	0.01	5.1 (−3)
		6	333.27	9.4 (−4)	0.01	9.4 (−4)	316.26	3.0 (−3)	0.01	3.0 (−3)
		7	349.58	3.9 (−4)	0.01	4.1 (−4)	334.54	1.4 (−3)	0.01	1.4 (−3)
		8	356.07	9.4 (−5)	-0.04	4.7 (−4)	342.29	5.2 (−4)	0.06	3.2 (−4)
3	1	0	−199.27	0	0.34	0	−238.26	9.6 (−4)	0.30	9.6 (−4)
		1	−6.17	0	0.29	0	−41.60	2.1 (−3)	0.24	2.1 (−3)
		2	141.10	1.9 (−2)	0.22	5.9 (−3)	110.78	1.4 (−2)	0.18	4.4 (−3)
		3	244.34	1.6 (−2)	0.13	6.0 (−3)	220.01	1.2 (−2)	0.08	4.9 (−3)
		4	308.82	1.1 (−2)	-0.05	4.5 (−3)	289.94	6.7 (−3)	-0.13	3.8 (−3)
		5	343.20	4.5 (−3)	-0.51	2.3 (−3)	327.91	1.4 (−3)	-0.78	2.0 (−3)
		6	354.81	1.3 (−3)	0.57	6.3 (−4)	340.80	2.3 (−3)	0.58	6.1 (−4)

TABLE EII: continued

3	0	0	−59.64	0			−85.77	1.0 (−3)		
		1	105.33	3.7 (−3)			80.41	3.8 (−2)		
		2	223.52	7.0 (−4)			202.04	2.2 (−2)		
		3	298.99	8.5 (−7)			281.49	9.9 (−3)		
		4	339.91	8.7 (−5)			325.11	3.4 (−3)		
		5	355.65	4.6 (−5)			341.85	6.9 (−4)		
ε			357.10				344.23			
5	5	0	−91.20	0	0.00	0	−167.35	1.6 (−3)	0.00	1.6 (−3)
		1	159.88	4.2 (−8)	0.00	1.3 (−8)	87.98	4.1 (−3)	0.00	4.1 (−3)
5	4	0	76.27	2.3 (−9)	0.00	2.8 (−9)	7.21	1.6 (−3)	0.00	1.6 (−3)
		1	306.77	3.8 (−5)	0.00	1.0 (−4)	241.80	4.4 (−3)	0.00	4.4 (−3)
5	3	0	220.14	1.1 (−5)	0.00	5.9 (−6)	158.68	1.1 (−3)	0.00	1.1 (−3)
5	2	0	335.74	2.6 (−4)	0.06	1.1 (−8)	281.77	1.2 (−3)	0.05	8.4 (−4)
ε			886.66				854.62			

[a] See footnote *a* in Table EI.
[b] All $\Gamma>0$ widths in the column are due to rotational predissociation.
[c] The red numbers in the column are widths due to pure vibrational predissociation ($E<\varepsilon_{11}$).

[1] W. P. Kraemer, V.Špirko, and O. Bludsky, Chem. Phys. **276**, 225 (2002).
[2] W. P. Kraemer and V. Špirko, Chem. Phys. **330**, 190 (2006).
[3] F. Mrugała and W.P. Kraemer, J. Chem. Phys. **122**, 224321 (2005).
[4] F. Mrugała and W. P. Kraemer, J. Chem. Phys. **138**, 104315 (2013).
[5] S. Kassi, A. Campargue, K. Pachucki, and J. Komasa, J. Chem. Phys. **136**, 184309 (2012).
[6] Part D of this material.